Solid state transformations of different stoichiometric forms of an organic salt formed by 5-sulfosalicylic acid and hexamethylenetetramine upon dehydration and rehydration

Qiang Fu, Xi-Kun Xu, Bao-Kai Liu, Fang Guo*
College of Chemistry, Liaoning University
Shenyang, 110036, China
fguo@lnu.edu.cn

Figures and Table

Fig. S9 Photomicrographs of $\mathbf{A_1B_2{\cdot}H_2O}$, showing the dehydration process at (a) 25 °C, (b) 160 °C, (c) 180 °C.

Fig. S16 2D fingerprint plot derived from the Hirshfeld surface.

Table S1 Hydrogen bonds of $\mathbf{A_1B_1 \cdot H_2O}$, $\mathbf{A_1B_1}$, $\mathbf{A_1B_2 \cdot H_2O}$, and $\mathbf{A_1B_2}$.

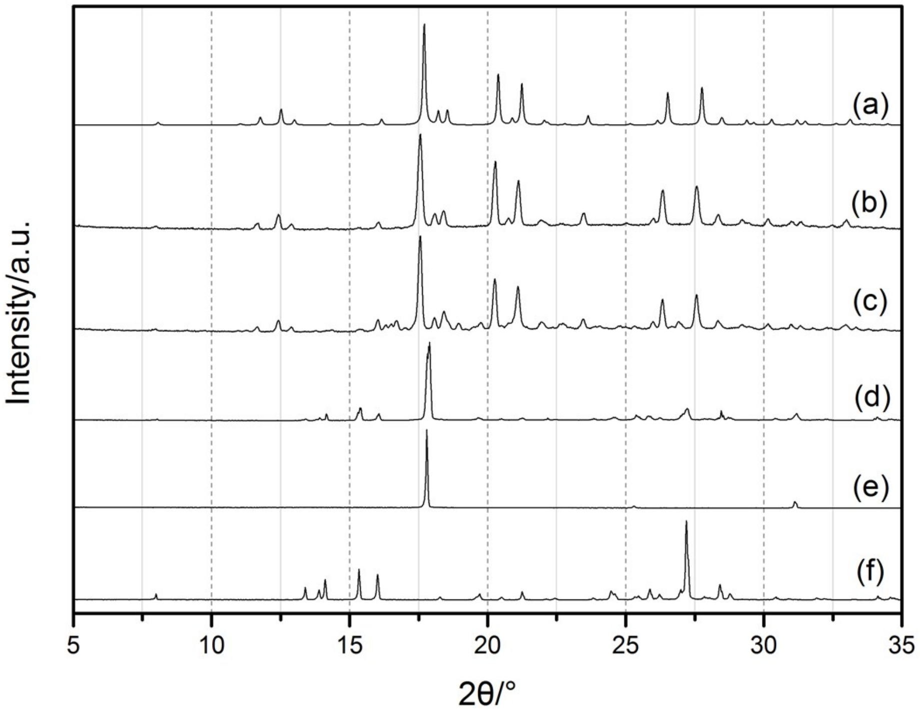

Fig. S1 PXRD patterns of $\mathbf{A_1B_1 \cdot H_2O}$ salts by ball milling in different times, (a) $\mathbf{A_1B_1 \cdot H_2O}$ simulated, (b) 120 s, (c) 60 s, (d) 20 s, (e) **B** and (f) **A**.

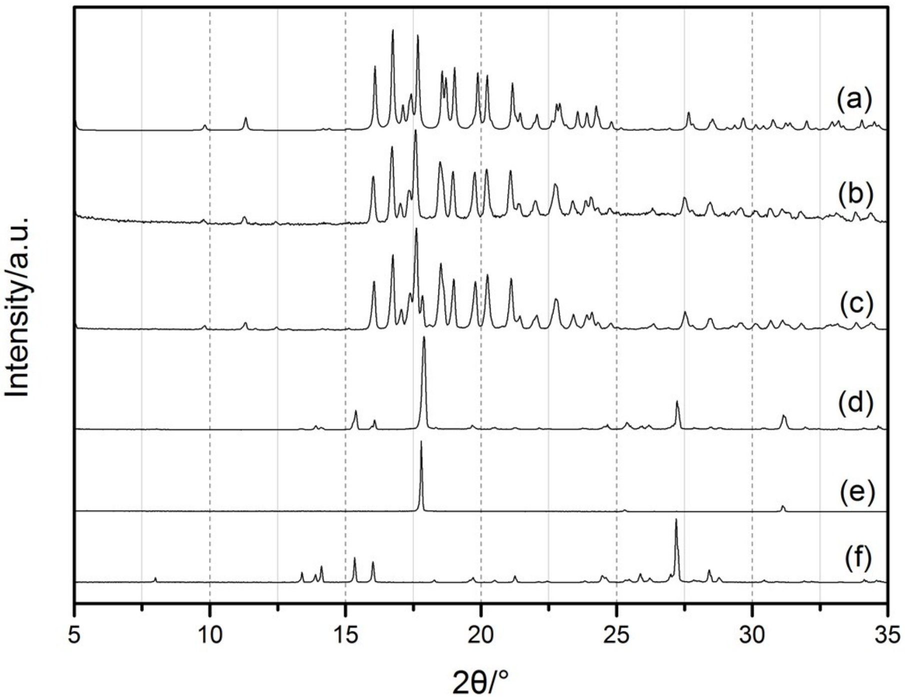

Fig. S2 PXRD patterns of $\mathbf{A_1B_2{\cdot}H_2O}$ salts by ball milling in different times, (a) $\mathbf{A_1B_2{\cdot}H_2O}$ simulated, (b) 120 s, (c) 60 s, (d) 20 s, (e) **B** and (f) **A**.

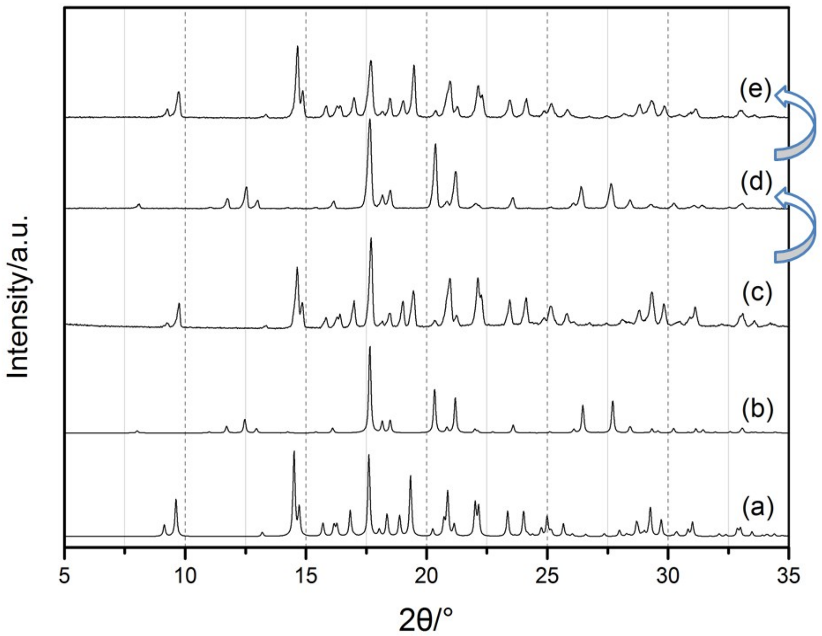

Fig. S3 Comparison of PXRD patterns for form $\mathbf{A_1B_1}$ before and after DVS: (a) $\mathbf{A_1B_1}$ simulation, (b) $\mathbf{A_1B_1{\cdot}H_2O}$ simulation, (c) $\mathbf{A_1B_1}$ before DVS (d) $\mathbf{A_1B_1}$ from the adsorption cycle (0-95% RH) DVS and (e) $\mathbf{A_1B_1{\cdot}H_2O}$ from the desorption cycle (95-0% RH).

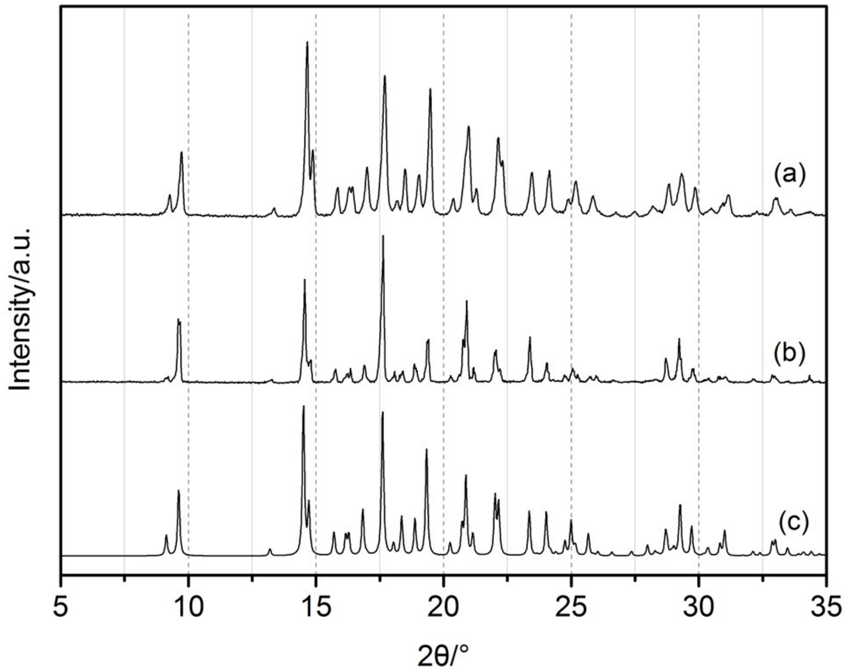

Fig. S4 Powder XRD of **A_1B_1** (a) heating product of **$A_1B_1·H_2O$** (b) single crystals (c) simulated.

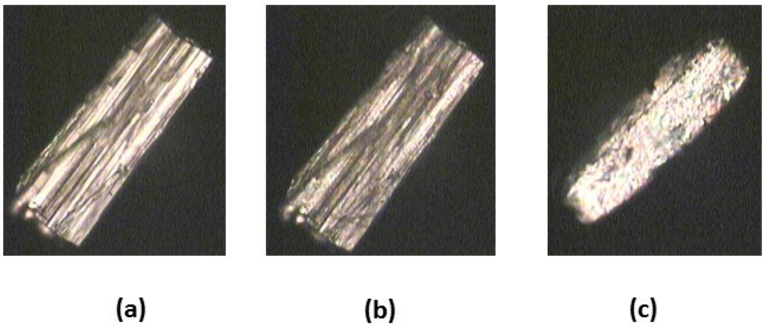
(a) (b) (c)

Fig. S5 Pictures taken on hot-stage micrograph showing the dehydration process of **$A_1B_1·H_2O$** at various temperatures: (a) 25 °C, (b) 130 °C and (c) 172 °C.

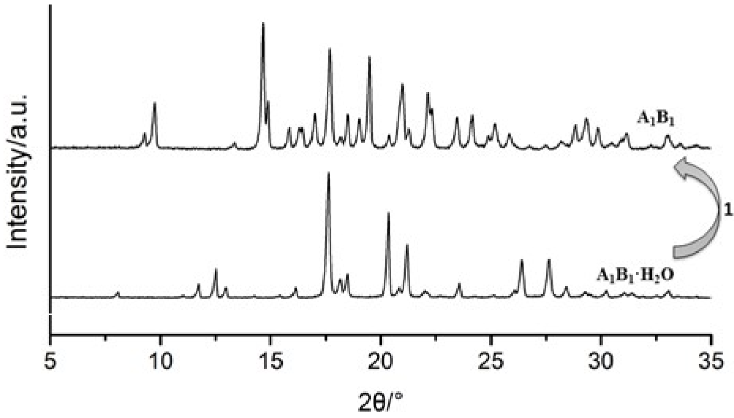

Fig. S6 The PXRD pattern of the crystalline material obtained after heating **$A_1B_1·H_2O$** to 130 °C.

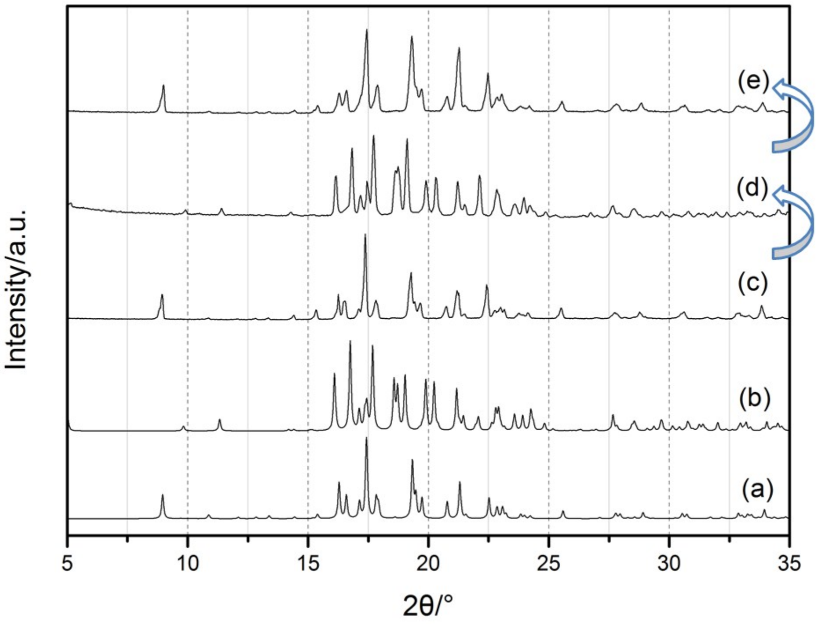

Fig. S7 Comparison of PXRD patterns for form $\mathbf{A_1B_2}$ before and after DVS: (a) $\mathbf{A_1B_2}$ simulation, (b) $\mathbf{A_1B_2{\cdot}H_2O}$ simulation, (c) $\mathbf{A_1B_2}$ before DVS (d) $\mathbf{A_1B_2}$ from the adsorption cycle (0-95% RH) DVS and (e) $\mathbf{A_1B_2{\cdot}H_2O}$ from the desorption cycle (95-0% RH).

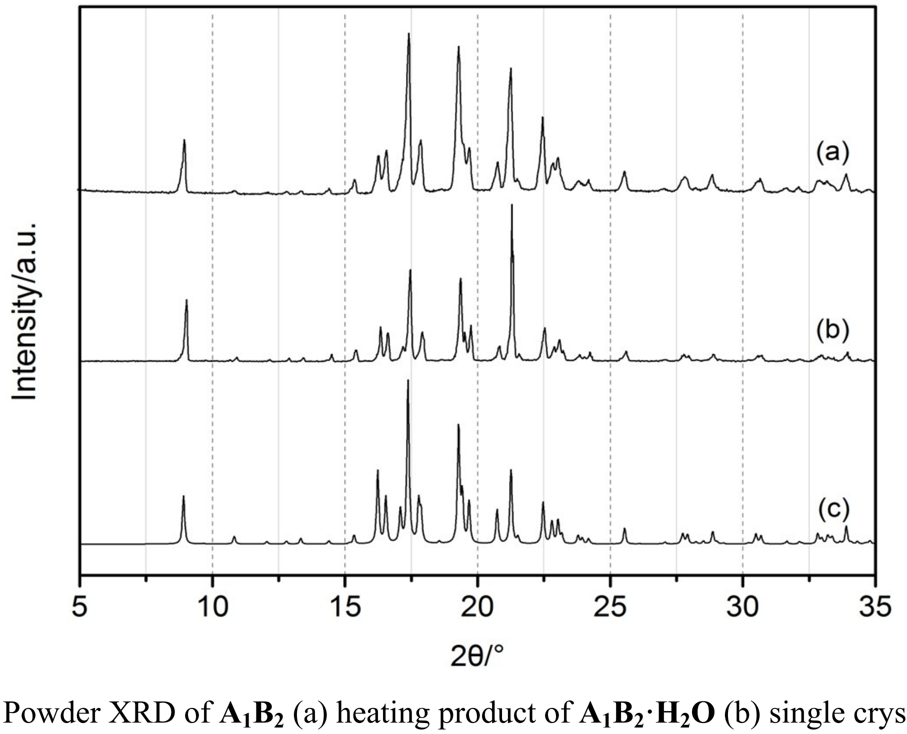

Fig. S8 Powder XRD of $\mathbf{A_1B_2}$ (a) heating product of $\mathbf{A_1B_2{\cdot}H_2O}$ (b) single crystals (c) simulated.

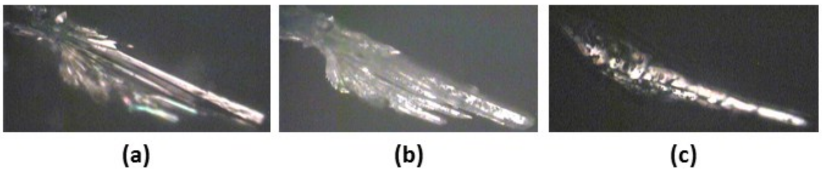

(a) (b) (c)

Fig. S9 Photomicrographs of **$A_1B_2 \cdot H_2O$**, showing the dehydration process at (a) 25 °C, (b) 160 °C and (c) 180 °C.

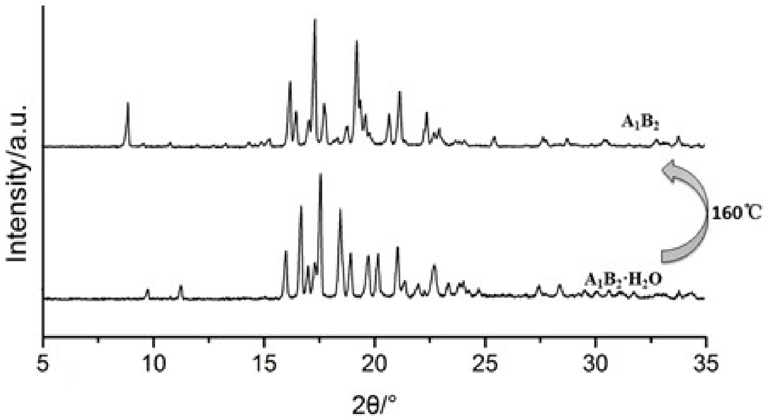

Fig. S10 The PXRD pattern of the crystalline material obtained after heating **$A_1B_2 \cdot H_2O$** to 160 °C.

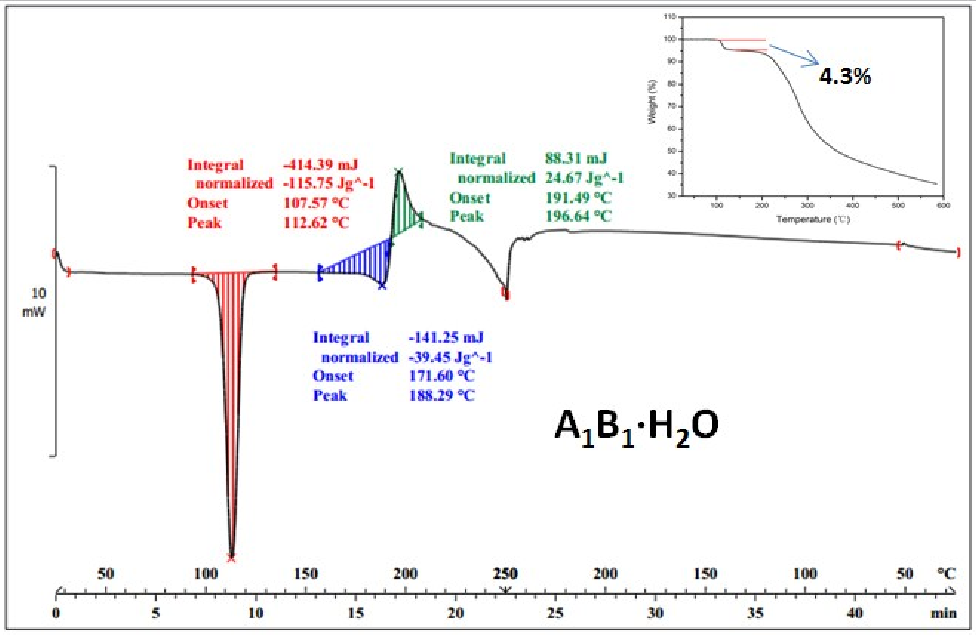

Fig. S11 DSC and TG curve of **$A_1B_1 \cdot H_2O$**.

$A_1B_1 \cdot H_2O$ shows two significant energy change. The first significant end`othermic peak corresponds to the transformation from **$A_1B_1 \cdot H_2O$** to **A_1B_1**, which is in accordance with the TGA analysis, in which the first weight loss in the temperature range from 107.6 °C to 122.8 °C corresponding to water loss (cal. 4.8%, exp. 4.3%), and the second endotherm-exothermic peaks occurs corresponding to melting-crystallization process. The onset temperature is 171.6 °C which corresponding to the melting point of **A_1B_1**

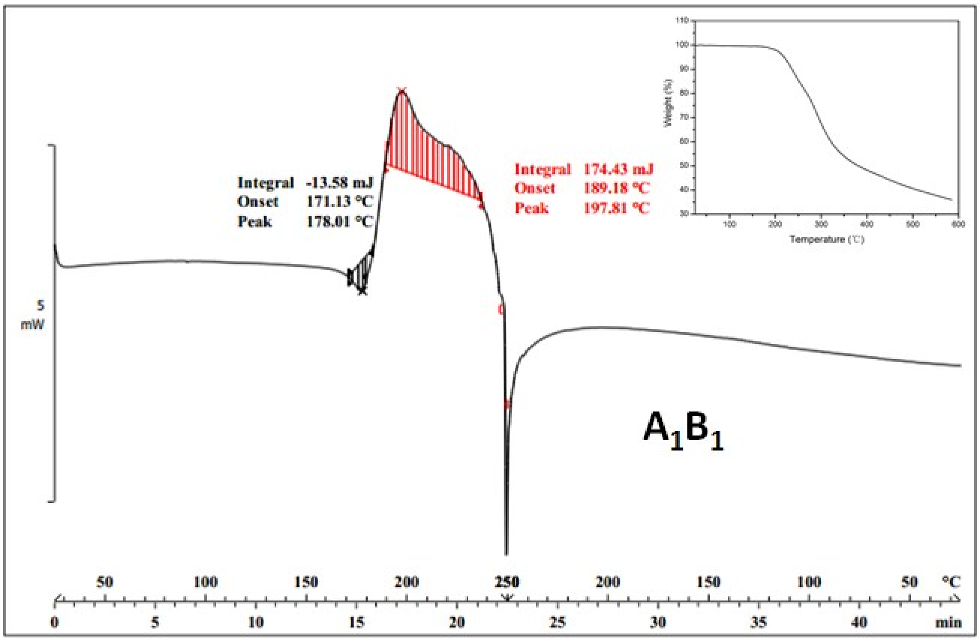

Fig. S12 DSC and TG curve of **A_1B_1**.

A_1B_1 shows an endothermic transition over the range 171.1 °C to 181.6 °C. The onset temperature is 171.1 °C which corresponding to the melting point of **A_1B_1**. Above this transition it observes an exothermic peak, which belongs to a classic melting-crystallization process.

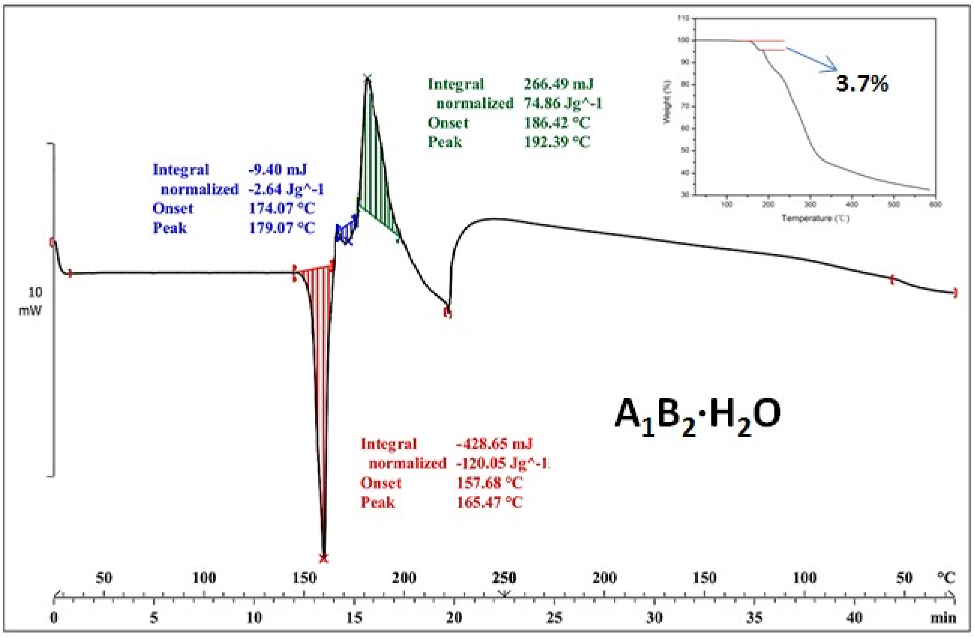

Fig. S13 DSC and TG curve of **$A_1B_2 \cdot H_2O$**.

$A_1B_2 \cdot H_2O$ shows a bit complicated curve. The first endothermic peak at 165.5 °C corresponds to the process of water loss, which is also observed in TGA curve (cal. 3.5%, exp. 3.7%). After 170 °C, **$A_1B_2 \cdot H_2O$** completely changed to **A_1B_2**. Then endotherm-exothermic peaks occur also corresponding to melting-crystallization process. The onset temperature is 174.1 ^{o}C which corresponding to the melting point of **A_1B_2**.

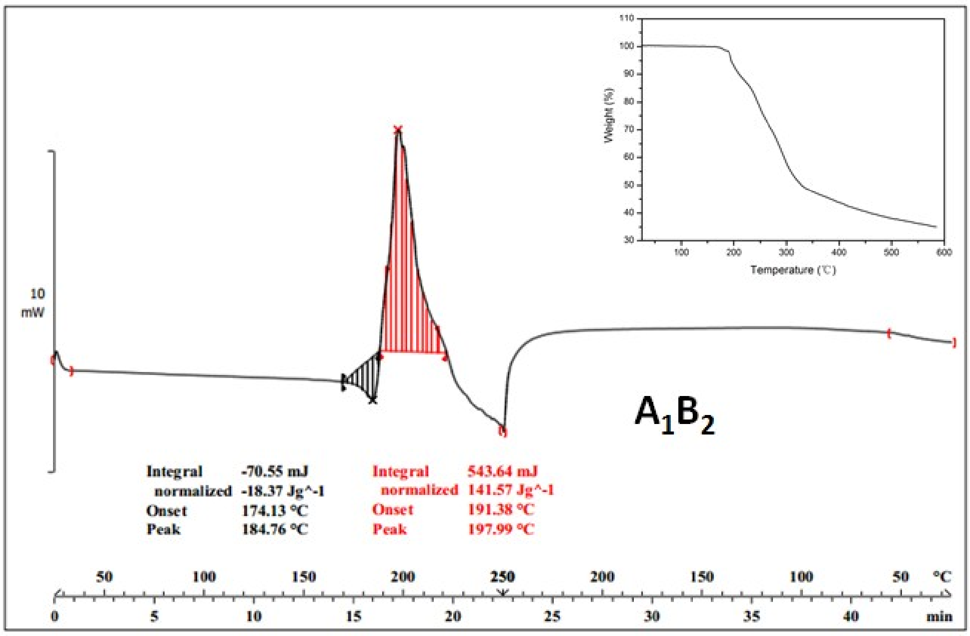

Fig. S14 DSC and TG curve of $\mathbf{A_1B_2}$.

$\mathbf{A_1B_2}$ has an endothermic reaction starting on 174.1 °C corresponding to melting point, and then follows an exothermic process corresponding to crystallization.

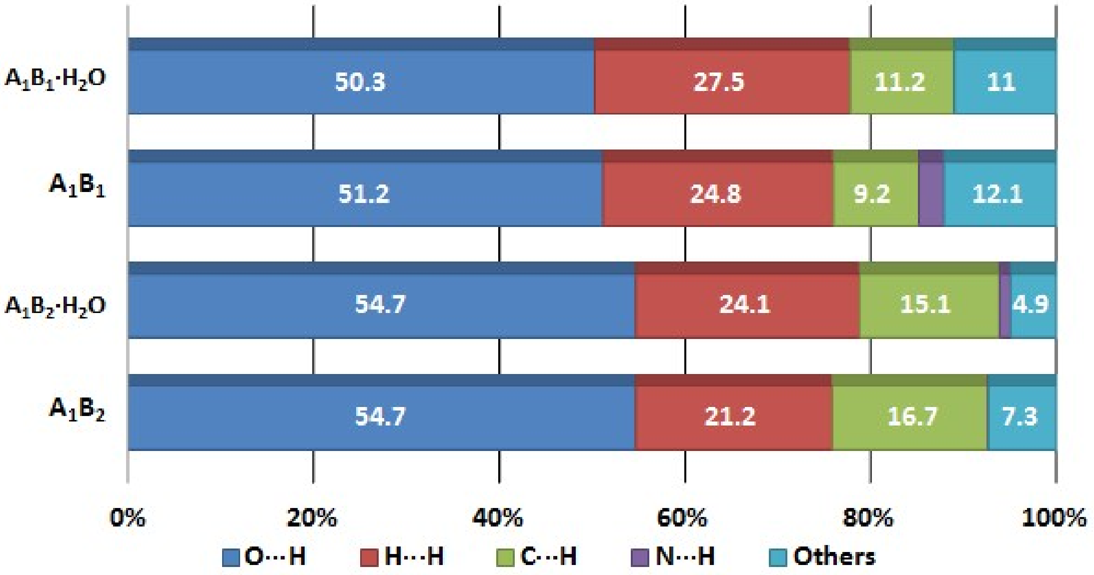

Fig. S15 Percentage contributions to the Hirshfeld surface area for the various close intermolecular contacts. Percentages are given on the histogram only for the major atom-type/atom-type contacts discussed in detail in the text.

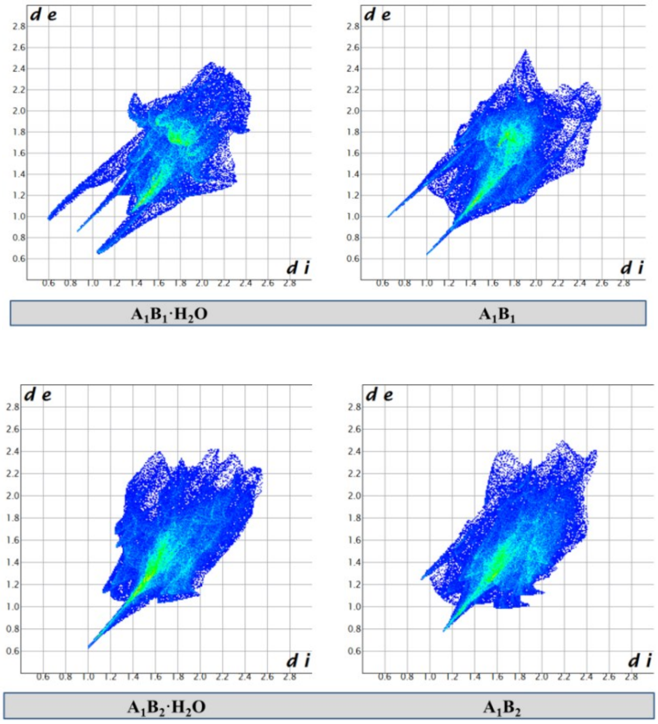

Fig. S16 2D fingerprint plot derived from the Hirshfeld surface.

In $\mathbf{A_1B_1{\cdot}H_2O}$ and $\mathbf{A_1B_1}$, **A** molecule can act as donors and acceptors simultaneously, thus two symmetric sharp spikes projecting along the diagonal of the plot can be seen in Hirshfeld surface (top), with one corresponding to the COOH as donors and the other corresponds to CO_2/SO_3 groups as acceptors. In $\mathbf{A_1B_1{\cdot}H_2O}$, the upper peak is associated with the interactions between COOH group (as donor) and water ($O–H\cdots O_{(water)}$), whereas the lower one is the interactions that COO/SO_3 groups as acceptors linking to N in **B** cations ($N_{(\mathbf{B})}–H\cdots O$) and water molecules ($O_{(water)}–H\cdots O$). For $\mathbf{A_1B_1}$, the upper peak is associated with the interactions between COOH donor and SO_3 group in another **A** anion ($O–H\cdots O_{(\mathbf{A})}$), whereas the lower peak represents the interactions with CO_2 and SO_3 as acceptors $O\cdots H–O_{(\mathbf{A})}$/$O\cdots H–N_{(\mathbf{B})}$. The difference between $\mathbf{A_1B_1{\cdot}H_2O}$ and $\mathbf{A_1B_1}$ is the middle sharp thin spike of $\mathbf{A_1B_1{\cdot}H_2O}$, representing the $H\cdots H$ interactions, which was further ascertained from the percentage contribution calculations to the Hirshfeld surface area for the various close intermolecular contacts (Fig. S15), in which $H\cdots H$ interaction are the subdominant contribution to Hirshfeld surface. It is worth mentioning that $H\cdots H$ interaction in $\mathbf{A_1B_1{\cdot}H_2O}$ accounts for 27.5%, which is highest among all the structures.

The derived fingerprint plots of $\mathbf{A_1B_2{\cdot}H_2O}$ and $\mathbf{A_1B_2}$ are relatively simple with only one spike projecting along the diagonal of the plot (bottom), which is in accordance with the fact that **A** molecules can only be acted as hydrogen bonding acceptors in these structures. Hirshfeld surface calculation reveals that these interactions in both structures are equally contributing 54.7% to all surface interactions. But it is obvious that the spike in $\mathbf{A_1B_2{\cdot}H_2O}$ is sharper and longer than that in $\mathbf{A_1B_2}$, which might due to the two kinds of interactions involved in $\mathbf{A_1B_2{\cdot}H_2O}$ ($N_{(\mathbf{B})}–H\cdots O$ and $O_{(water)}–H\cdots O$), whereas only one kind of interaction in $\mathbf{A_1B_2}$ ($N_{(\mathbf{B})}–H\cdots O$).

Table S1 Hydrogen bonds of $\mathbf{A_1B_1{\cdot}H_2O}$, $\mathbf{A_1B_1}$, $\mathbf{A_1B_2{\cdot}H_2O}$, and $\mathbf{A_1B_2}$.

D-H···A	D-H (Å)	H···A(Å)	D···A(Å)	∠(DHA)°	Symmetry
$A_1B_1 \cdot H_2O$					
O3-H3A···O1 (i)	0.849	1.842	2.623	152.16	x, y, z
N2-H2B···O1 (ii)	0.849	2.393	2.973	126.07	-0.5+x,y,1.5-z
O2-H2A···Ow (iii)	0.898	1.644	2.539	174.56	x,y,z
N2-H2B···Ow (iv)	0.849	2.126	2.850	143.03	-0.5+x,y,1.5-z
A_1B_1					
O3-H3A···O2 (i)	0.910	1.823	2.637	147.62	x, y, z
N1-H1N···O2 (ii)	0.912	2.263	2.913	127.87	1-x, 2-y,- z
N1-H1N···O5 (iii)	0.912	2.180	2.970	144.54	1+x, y, z
O1-H1O···O4 (iv)	0.895	1.715	2.599	168.99	1-x, 2-y, -z
$A_1B_2 \cdot H_2O$					
O3-H3A···O2 (i)	0.938	1.595	2.493	158.83	x, y, z
N4-H4N···O1w (ii)	0.890	2.069	2.822	141.72	-1+x, y, -1+z
O1w-H1w1···O5 (iii)	0.871	1.924	2.792	174.28	x, y, z
O1w-H1W2...O6(iv)	0.881	1.863	2.741	173.95	1+x, y, z
N5-H5...O1(v)	0.967	1.680	2.646	177.09	1+x, 0.5-y, -0.5+z
N4-H4N···O1w (vi)	0.890	2.289	2.927	128.50	1-x,-y,1-z
A_1B_2					
O3-H3···O2 (i)	0.825	1.742	2.508	153.65	x, y, z
N5-H5···O4 (ii)	0.815	2.160	2.773	132.01	-1+x, y, z
N1-H1···O1(iii)	0.815	2.101	2.798	143.46	x, y, z
N5-H5···O1(iv)	0.846	2.057	2.772	141.86	-0.5+x, 0.5-y, -z
N1-H1···O4(v)	0.846	2.299	2.931	131.71	-0.5+x, 0.5-y, -z